Laminating solution-processed silver nanowire mesh electrodes onto solid-state dye-sensitized solar cells

Brian E. Hardin [a], Whitney Gaynor [a], I-Kang Ding [a], Seung-Bum Rim [b], Peter Peumans [b], Michael D. McGehee [a],*

[a] Department of Materials Science and Engineering, Stanford University, Stanford, CA 94305, USA
[b] Department of Electrical Engineering, Stanford University, Stanford, CA 94305, USA

ABSTRACT

Solution processed silver nanowire meshes (Ag NWs) were laminated on top of solid-state dye-sensitized solar cells (ss-DSCs) as a reflective counter electrode. Ag NWs were deposited in <1 min and were less reflective compared to evaporated Ag controls; however, AgNW ss-DSC devices consistently had higher fill factors (0.6 versus 0.69), resulting in comparable power conversion efficiencies (2.7%) compared to thermally evaporated Ag control (2.8%). Laminated Ag NW electrodes enable higher throughput manufacturing and near unity material usage, resulting in a cheaper alternative to thermally evaporated electrodes.

© 2011 Elsevier B.V. All rights reserved.

1. Introduction

Dye-sensitized solar cells (DSCs) [1–3] are an emerging photovoltaic technology on the verge of commercialization with devices based on iodide/tri-iodide liquid electrolytes exceeding power conversion efficiencies of 11% [4]. Liquid DSCs can be made via high throughput processes because liquid based DSCs do not require vacuum deposition techniques during assembly. However, two pieces of fluorine doped tin oxide (FTO) covered glass are often used as the front and back electrodes, which represent a significant fraction of production costs for the liquid DSC. Solid-state dye-sensitized solar cells (ss-DSC), which replace the liquid electrolyte with a solid organic hole conductor (e.g. spiro-OMeTAD), have two significant manufacturing advantages over the liquid-electrolyte based DSCs: (1) solid hole conductors are easier to package and potentially more stable than volatile liquid electrolytes and (2) ss-DSCs require only one piece of transparent conducting glass used as

the front electrode. However, the counter electrode of ss-DSCs are deposited via thermal evaporation of Au or Ag [5,6]. It is highly desirable to develop alternative deposition techniques to deposit reflective counter electrodes for ss-DSCs. Several groups have recently replaced thermally evaporated counter electrodes by spray coating Ag nanoparticles in solution on top of organic photovoltaic cells and achieved comparable performance [7,8]. Ag nanoparticle films deposited via spray coating usually require a 150–200 °C sintering step [9], which can crystallize the spiro-OMeTAD and dissociate the dye from the titania. It is desirable to develop Ag printing techniques that can be performed at room temperature.

It has recently been shown that films of Ag nanowires can be transferred through lamination to serve as a transparent top electrodes in organic photovoltaic devices [10,11]. Ag NWs films are first made by drop-cast from a liquid suspension in air to a host substrate and annealed to achieve sheet resistances comparable to those of transparent conducting oxides [11]. The Ag NWs films are then transferred from the host substrate to the solar cell by mechanical pressing, as shown in Fig. 1A. Thin layers of
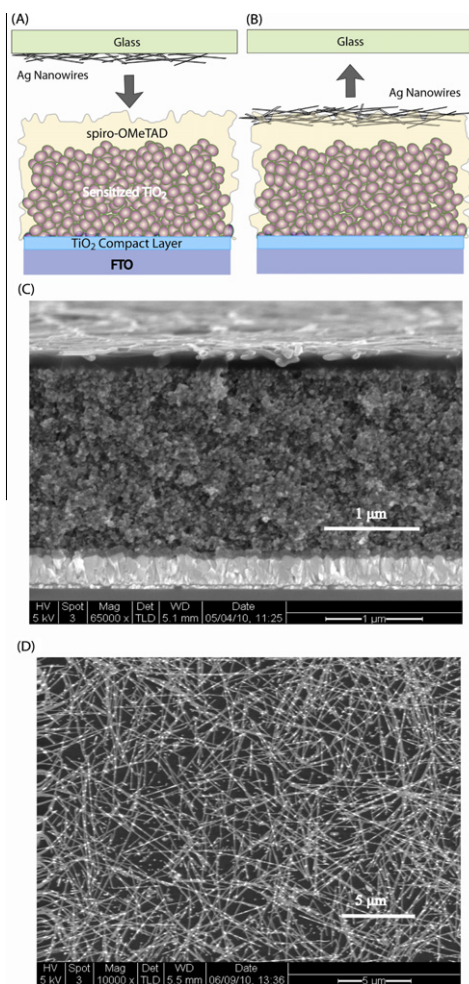
Fig. 1. Device schematic of dye sensitized solar cell (A) before and (B) after Ag NW lamination. (C) SEM side view image (65,000× magnification, 1 µm scale bar) and (D) SEM top view image (10,000× magnification, 5 µm scale bar) of solid-state DSC after Ag NW lamination.

Ag NWs show high transparency in the solar spectrum, have low sheet resistance, and can be processed with high throughput. As the nanowire concentration of the film increases, the transmission decreases and the films become more reflective. In this letter, we show that thick Ag NW meshes can be deposited on top of ss-DSCs as the reflective counter electrode without an annealing step producing comparable power conversion efficiencies versus the evaporated Ag control devices.

ss-DSCs have an empirically optimized titania film thickness of ~2.2 µm (versus >10 µm for liquid DSCs); which is likely due to higher rates of recombination [12,13]. Despite the thinner device architecture, which lowers overall light absorption, ss-DSCs have recently achieved maximum power conversion efficiencies of 6.1% [14]. ss-DSCs have the potential to match or exceed liquid based DSC performance by developing higher molar extinction coefficient dyes for increased light absorption [15–17], hole conductors with lower HOMO levels, new architectures to increase light harvesting [18–23], and tandem devices.

2. Experimental

2.1. Solid-state dye-sensitized solar cell device fabrication

Solid-state DSCs are shown schematically in Fig. 1A. ss-DSCs consist of Flourine doped SnO_2 conducting glass (Hartford Glass TEC 15) which was partially etched using zinc powder and HCl (12%) then cleaned by sonication sequentially in 10% extran, acetone, isopropanol, and water. A 50 nm compact TiO_2 layer was deposited via aerosol spray pyrolysis using air as the carrier gas [24]. Mesoporous titania films were deposited via doctor blading of commercially available paste (Dyesol 18NR-T) and slowly heated to 500 °C for 30 min in air. It should be noted, that TiO_2 paste deposition was performed in a laminar flow hood to minimize dust contamination that can affect the Ag NW transfer. Films were subsequently treated in 0.02 M $TiCl_4$ aqueous solution overnight at room temperature [25]. Samples were then heated to 450 °C for 10 min cooled to approximately 80 °C and immersed in 0.3 mM of Z907 (Solaronix SA) in a 1:1 mixture of acetonitrile and tert-butyl alcohol for 12–18 h. The organic hole conductor solution was made by dissolving 72 mg of 2,2′,7,7′tetrakis-(N,N-di-p-methoxyphenylamine)-9,9′-spirobifluorene (spiro-OMeTAD) in 400 µl of chlorobenzene and then adding 7 µl of tert-butylpyridine and 15 µl of 0.6 M bis(trifluoromethane)sulfonamide lithium salt (Fluka) in acetonitrile. The doped spiro-OMeTAD solution was deposited on the substrate and allowed to infiltrate the TiO_2 for 30 s prior to spin coating (2000 RPM for 40 s) and dried in a dessicator for several hours. Ag counter electrodes (200 nm) for the control devices were evaporated at 2×10^{-6} torr on half of the substrate.

2.2. Silver nanowire synthesis and lamination onto DSC

Silver nanowires were synthesized by reducing Ag nitrate in the presence of poly(vinyl pyrrolidione) in ethylene glycol which resulted in Ag NWs that were on average 8.7 µm long and have 103 nm diameters [11,26]. To create films on the host substrate, Ag NWs were deposited from methanol onto coverslip glass and annealed at 180 °C to fuse the junctions between the wires and enhance conductivity [10,11,27]. The Ag NW films were then pressed onto the spiro-OMeTAD at a pressure of 1.6×10^4 psi for approximately 30 s, as illustrated in Fig. 1A and B. Care should be taken during lamination to remove any debris on the press and align the press to consistently apply pressure across the glass surface; inconsistent pressure can cause substrate cracking. Laminated Ag NW films were roughly 2–4 nanowires thick (100–200 nm) as shown in the SEM image in Fig. 1C. During lamination >95% of the Ag NWs are transferred to the ss-DSC substrate. The overall surface coverage is relatively sparse as shown in Fig. 1D. ImageJ software was used to analyze the SEM image and determined that approximately 59% of the spiro-OMeTAD surface is covered by AgNWs. A four-point probe measurement was used to determine a sheet resistance of 4.5 Ω/□ for AgNWs counter electrode versus 1.3 Ω/□ for 200 nm of evaporated silver on inert
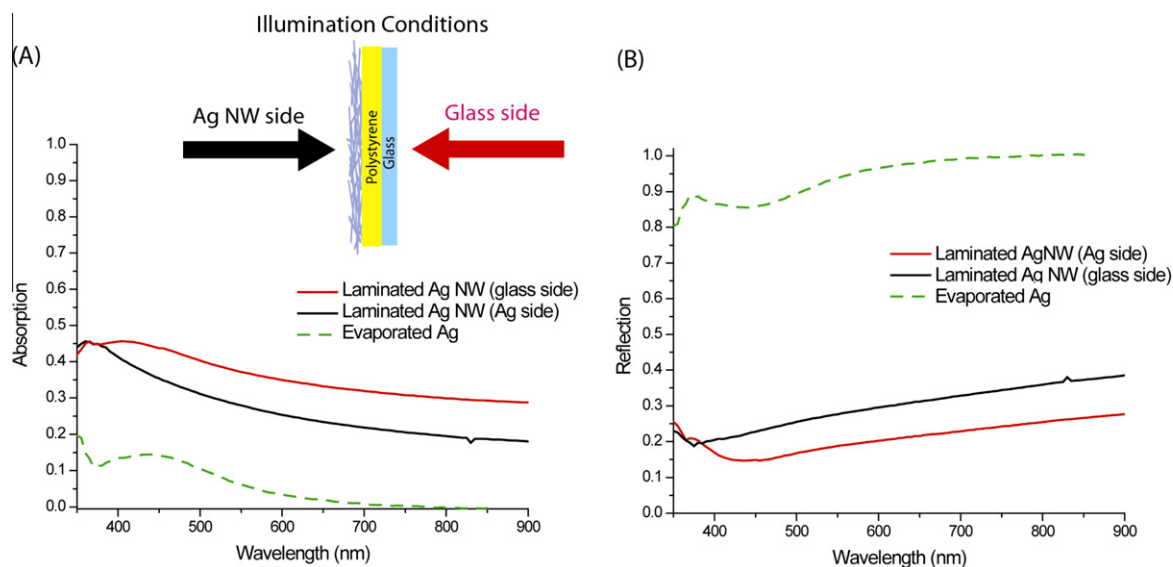
Fig. 2. Specular and diffuse (A) Absorption and (B) reflection of evaporated Ag versus laminated Ag NW electrodes on polystyrene/glass substrate under various illumination conditions described in the inset.

polystyrene films. The counter electrode makes a relatively small contribution to the series resistance which is dominated by the FTO (15 $\Omega/\square$) and the internal resistance of the doped spiro-OMeTAD. It should be noted, that Ag NWs were laminated on the same substrate as evaporated Ag to ensure the most accurate comparison.

3. Results and discussion

For measurements to determine the optical properties of the counter electrodes, Ag was evaporated and Ag NWs were pressed into a thin layer (<100 nm) of polystyrene on a glass slide as shown in the inset of Fig. 2. Polystyrene is a wide band gap polymer with negligible absorption in the visible and near-infrared portion of the spectrum. Absolute (i.e. specular and diffuse) light absorption (Fig. 2A) and transmission were measured with an integrating sphere (Labsphere) with methods previously described [28]. The absolute reflection (Fig. 2B) was calculated from the absorption and transmission values (i.e. $R = 1 - T - A$). The absorption of Ag NWs is dependent upon the illumination condition; Ag NWs absorb more light when illuminated from the glass/polystyrene side (red solid)[1] versus the Ag NW side (black solid) as shown in Fig. 2A. The increase in absorption may be caused by increased light scattering due to changes in the Ag NW morphology during lamination and via total internal reflections inside the polystyrene/glass. During lamination, the cylindrically shaped silver nanowires penetrate into the soft polymer surface creating a rough, scattering interface on the polystyrene side. However, the portion of the Ag NW touching the host substrate is flattened and becomes relatively smooth (Fig. 1C) reducing light scattering. Secondly, light scattered in the polystyrene, which has an index of

refraction of approximately 1.55, can undergo total internal reflection increasing the optical path length and increasing overall light absorption by Ag NWs. Evaporated Ag (green dash) is only slightly absorptive and is highly reflective throughout the spectrum for both illumination directions. The variation in reflection between Ag NWs and evaporated Ag films is primarily related to higher light absorption by the Ag NWs and the low surface density of Ag NWs compared to the unity surface coverage of evaporated Ag.

Fig. 3A displays the total light absorption of all layers in ss-DSC devices using Ag NWs and evaporated Ag contacts illuminated through the FTO side. Spiro-OMeTAD dominates light absorption inside the ss-DSC from 350 to 425 nm. Both the evaporated Ag and Ag NW ss-DSCs have similar absorption profiles in the region where the sensitizing dye absorbs most strongly (425–550 nm). At the peak absorption of the Z907 (525 nm), roughly 80% of the light is absorbed by the control versus 71% for the Ag NW ss-DSCs. Most of the loss in absorption is due to transmission through the device; specular transmission measurements (not shown) reveal that 15% of the light at 525 nm is transmitted through the Ag NW ss-DSC. In the red/near-infrared portion of the spectrum, the Ag NW ss-DSCs have overall higher absorption due to Ag NW absorption that does not contribute to the photocurrent. It should be noted that the Ag NW ss-DSC absorption profile is smoother and does not contain the interference effects typically seen with evaporated electrodes. Because these measurements were taken on the same substrate, the smooth profile further strengthens our hypothesis that pressing nanowires into the spiro-OMeTAD overlayer roughens the rear interface, increasing scattering off of the back contact and reducing interference effects.

External quantum efficiency (EQE) measurements were performed at a chopping frequency of 45 Hz using a Stanford Research System lock-in amplifier (Model SR830) under white light bias equivalent to 10% sun. The

---

[1] For interpretation of the references to colour in Figs. 1 and 2, the reader is referred to the web version of this article.
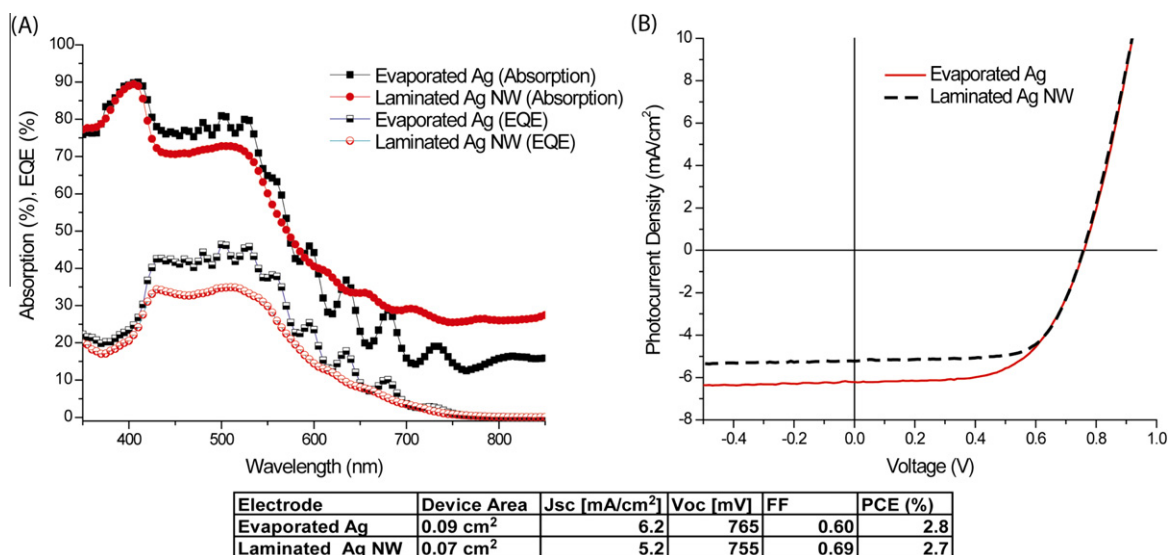
Fig. 3. (A) Total light absorption and external quantum efficiency plots of solid-state dye-sensitized solar cells made with evaporated Ag and laminated Ag NW counter electrodes. (B) Photocurrent density versus voltage (JV) plot of ss-DSCs with Ag NW counter electrode (red line) versus evaporated Ag control (dashed black line). PV device characteristics are shown in the figure inset.

EQE, shown in Fig. 3A, scales with light absorption and explains the correspondingly lower photocurrent of Ag NW ss-DSCs versus the control shown in Fig. 3B. Ag NW devices have comparable power conversion efficiency (2.7%) versus the control ss-DSC (2.8%). Ag NW devices have lower short-circuit current density (Jsc), due to a lower reflectivity, but consistently displayed higher fill factors (FF) and behaved differently during light soaking. Evaporated Ag devices initially had very low fill factors (0.4–0.45) and required >15 min of light soaking (100% sun) under +1 V bias to dramatically increase the fill factor (0.55–0.60). Ag NW based devices had significantly higher initial fill factors (0.57–0.65) that increased slightly over <5 min of light soaking to (0.62–0.69). It should be noted that FF ranges were based on five devices that contained an equal number of evaporated Ag and Ag NW electrodes. Despite the slightly higher sheet resistance of Ag NW electrodes, the overall series resistance, which can be approximated as the slope of the JV curves at far forward bias, is nominally the same for both devices. The spiro-OMeTAD overlayer is known to increase the series resistance and decrease the fill factor of ss-DSCs [29]. Pressed Ag NWs penetrate into the 150–200 nm spiro-OMeTAD overlayer, which we believe helps lower the effective series resistance within the spiro-OMeTAD layer, compensating for the higher sheet resistance of the Ag NWs. In addition, Ag NWs films are fabricated and stored in air, which creates a thin silver oxide layer on the surface that increases the work function and may improve charge collection. The work function of Ag, at 4.4 eV, is significantly higher than the HOMO level of spiro-OMeTAD (5.2 eV), which requires large band bending or Fermi-level pinning [30] at the spiro-OMeTAD/Ag interface for good electrical contact. However, silver oxide (Ag₂O) has a work function of 5.1 eV and often exhibits p-type conductivity [31], which would act as an ideal charge collector with minimal recombination losses at this interface [5]. Evaporated Ag electrodes, however, are deposited in vacuum and may require time to allow for oxygen to diffuse and oxidize Ag at the metal/spiro-OMeTAD interface, possibly explaining the requirement of longer light soaking times to achieve a higher FF. A complete explanation of the effects of light soaking on solid-state DSCs is beyond the scope of this work and will be discussed in a future study.

4. Discussion and conclusion

Reflectivity, and thus overall power conversion efficiency of metal nanowire based electrodes, can be improved by developing new procedures to deposit more nanowires on the ss-DSC. Laminated Ag NWs are limited due to the pressing procedure, as each wire must come into contact with the soft hole conductor to be transferred. Wire meshes that are too thick cannot be completely transferred to another substrate. Directly spray coating or doctor blading NWs onto the cell could increase the overall surface concentration. These techniques would require solvents that do not dissolve the spiro-OMeTAD and a low temperature sintering step to prevent degradation of the ss-DSC. Laminating Ag nanoparticle films, which can be made into more densely packed films, may also result in more reflective films [9,32].

To the best of our knowledge, reflective silver nanowire meshes represent the first replacement of evaporated metal counter electrodes used in solid-state DSCs. This work demonstrates the general feasibility of laminating Ag NWs on ss-DSCs and achieves comparable device performance with standard thermally deposited Ag electrodes but with the potential for high throughput processing and unity material usage. This work may be extended to

semi-transparent Ag NW electrodes for ss-DSCs. Semi-transparent Ag NW meshes could be used as the front contact on glass-free, flexible ss-DSCs which use titania nanoparticles on metal foil [33] and also as an intermediary electrode in a tandem ss-DSC architecture. Finally, it should be noted that Ag NWs are dissolved by iodide based electrolytes, but may be implemented in liquid DSCs that use organic electrolytes [34,35].

Acknowledgements

References

[1] B. O'Regan, M. Grätzel, A low-cost, high-efficiency solar cell based on dye-sensitized colloidal TiO$_2$ films, Nature 353 (1991) 737–740.
[2] L.M. Peter, Dye-sensitized nanocrystalline solar cells, Physical Chemistry Chemical Physics 9 (2007) 2630–2642.
[3] A. Hagfeldt, M. Grätzel, Molecular photovoltaics, Accounts of Chemical Research 33 (2000) 269–277.
[4] Y. Cao, Y. Bai, Q. Yu, Y. Cheng, S. Liu, D. Shi, F. Gao, P. Wang, Dye-sensitized solar cells with a high absorptivity ruthenium sensitizer featuring a 2-(hexylthio)thiophene conjugated bipyridine, The Journal of Physical Chemistry C 113 (2009) 6290–6297.
[5] H.J. Snaith, A.J. Moule, C. Klein, K. Meerholz, R.H. Friend, M. Grätzel, Efficiency enhancements in solid-state hybrid solar cells via reduced charge recombination and increased light capture, Nano Letters 7 (2007) 3372–3376.
[6] R.A. Street, W.S. Wong, S.E. Ready, M.L. Chabinyc, A.C. Arias, S. Limb, A. Salleo, R. Lujan, Jet printing flexible displays, Materials Today 9 (2006) 32–37.
[7] C. Girotto, B.P. Rand, S. Steudel, J. Genoe, P. Heremans, Nanoparticle-based, spray-coated silver top contacts for efficient polymer solar cells, Organic Electronics 10 (2009) 735–740.
[8] S.K. Hau, H.-L. Yip, K. Leong, A.K.Y. Jen, Spraycoating of silver nanoparticle electrodes for inverted polymer solar cells, Organic Electronics 10 (2009) 719–723.
[9] J.R. Greer, R.A. Street, Thermal cure effects on electrical performance of nanoparticle silver inks, Acta Materialia 55 (2007) 6345–6349.
[10] W. Gaynor, J.-Y. Lee, P. Peumans, Fully solution-processed inverted polymer solar cells with laminated nanowire electrodes, ACS Nano 4 (2009) 30–34.
[11] J.-Y. Lee, S.T. Connor, Y. Cui, P. Peumans, Solution-processed metal nanowire mesh transparent electrodes, Nano Letters 8 (2008) 689–692.
[12] L. Schmidt-Mende, S.M. Zakeeruddin, M. Gratzel, Efficiency improvement in solid-state-dye-sensitized photovoltaics with an amphiphilic ruthenium-dye, Applied Physics Letters 86 (2005) 13504.
[13] L. Schmidt-Mende, H.J. Snaith, Advances in liquid-electrolyte and solid-state dye-sensitized solar cells, Advanced Materials 19 (2007) 3187–3200.
[14] X. Liu, W. Zhang, S. Uchida, L. Cai, B. Liu, S. Ramakrishna, An efficient organic-dye-sensitized solar cell with in situ polymerized poly(3,4-ethylenedioxythiophene) as a hole-transporting material, Advanced Materials 22 (2010) E1–E6.
[15] R. Li, J. Liu, N. Cai, M. Zhang, P. Wang, Synchronously reduced surface states, charge recombination, and light absorption length for high-performance organic dye-sensitized solar cells, The Journal of Physical Chemistry B 114 (2010) 4461–4464.
[16] A. Mishra, M.K.R. Fischer, P. Bäuerle, Metal-free organic dyes for dye-sensitized solar cells: from structure: property relationships to design rules, Angewandte Chemie International Edition 48 (2009) 2474–2499.
[17] S. Ardo, G.J. Meyer, Photodriven heterogeneous charge transfer with transition-metal compounds anchored to TiO$_2$ semiconductor surfaces, Chemical Society Reviews 38 (2009) 115–164.
[18] B.E. Hardin, E.T. Hoke, P.B. Armstrong, J.-H. Yum, P. Comte, T. Torres, J.M.J. Frechet, M.K. Nazeeruddin, M. Gratzel, M.D. McGehee, Increased light harvesting in dye-sensitized solar cells with energy relay dyes, Natural Photon 3 (2009) 406–411.
[19] J.H. Yum, B.E. Hardin, S.J. Moon, E. Baranoff, F. Nüesch, M.D. McGehee, M. Grätzel, M.K. Nazeeruddin, Panchromatic response in solid-state dye-sensitized solar cells containing phosphorescent, Angewandte Chemie International Edition 48 (2009) 9277–9280.
[20] G.K. Mor, J. Basham, M. Paulose, S. Kim, O.K. Varghese, A. Vaish, S. Yoriya, C.A. Grimes, High-efficiency forster resonance energy transfer in solid-state dye sensitized solar cells, Nano Letters 10 (2010) 2387–2394.
[21] J.A. Chang, J.H. Rhee, S.H. Im, Y.H. Lee, H.-j. Kim, S.I. Seok, M.K. Nazeeruddin, M. Grätzel, High-performance nanostructured inorganic-organic heterojunction solar cells, Nano Letters 10 (2010) 2609–2612.
[22] M. Shalom, J. Albero, Z. Tachan, E. Martinez-Ferrero, A. Zaban, E. Palomares, Quantum dot-dye bilayer-sensitized solar cells: breaking the limits imposed by the low absorbance of dye monolayers, The Journal of Physical Chemistry Letters 1 (2010) 1134–1138.
[23] S. Buhbut, S. Itzhakov, E. Tauber, M. Shalom, I. Hod, T. Geiger, Y. Garini, D. Oron, A. Zaban, Built-in quantum dot antennas in dye-sensitized solar cells, ACS Nano 4 (2010) 1293–1298.
[24] L. Kavan, M. Grätzel, Highly Efficient semiconducting TiO$_2$ photoelectrodes prepared by aerosol pyrolysis, Electrochimica Acta 40 (1995) 643–652.
[25] P.M. Sommeling, B.C. O'Regan, R.R. Haswell, H.J.P. Smit, N.J. Bakker, J.J.T. Smits, J.M. Kroon, J.A.M. van Roosmalen, Influence of a TiCl$_4$ post-treatment on nanocrystalline TiO$_2$ films in dye-sensitized solar cells, Journal of Physical Chemistry B 110 (2006) 19191–19197.
[26] A. Tao, F. Kim, C. Hess, J. Goldberger, R. He, Y. Sun, Y. Xia, P. Yang, Langmuir-blodgett silver nanowire monolayers for molecular sensing using surface-enhanced raman spectroscopy, Nano Letters 3 (2003) 1229–1233.
[27] J.-Y. Lee, S.T. Connor, Y. Cui, P. Peumans, Semitransparent organic photovoltaic cells with laminated top electrode, Nano Letters 10 (2010) 1276–1279.
[28] J. Zhu, Z. Yu, G.F. Burkhard, C.-M. Hsu, S.T. Connor, Y. Xu, Q. Wang, M. McGehee, S. Fan, Y. Cui, Optical absorption enhancement in amorphous silicon nanowire and nanocone arrays, Nano Letters 9 (2008) 279–282.
[29] I.K. Ding, N. Tétreault, J. Brillet, B.E. Hardin, E.H. Smith, S. Rosenthal, F. Sauvage, M. Grätzel, M.D. McGehee, Pore-filling of spiro-OMeTAD in solid-state dye sensitized solar cells: quantification, mechanism, and consequences for device performance, Advanced Functional Materials 19 (2009) 2431–2436.
[30] C. Tengstedt, W. Osikowicz, W.R. Salaneck, I.D. Parker, C.-H. Hsu, M. Fahlman, Fermi-level pinning at conjugated polymer interfaces, Applied Physics Letters 88 (2006) 053502–053503.
[31] U. Kumar Barik, S. Srinivasan, C.L. Nagendra, A. Subrahmanyam, Electrical and optical properties of reactive DC magnetron sputtered silver oxide thin films: role of oxygen, Thin Solid Films 429 (2003) 129–134.
[32] V. Sholin, S.A. Carter, R.A. Street, A.C. Arias, High work function materials for source/drain contacts in printed polymer thin film transistors, Applied Physics Letters 92 (2008) 063307.
[33] S. Ito, N.-L.C. Ha, G. Rothenberger, P. Liska, P. Comte, S.M. Zakeeruddin, P. Pechy, M.K. Nazeeruddin, M. Grätzel, High-efficiency (7.2%) flexible dye-sensitized solar cells with Ti-metal substrate for nanocrystalline–TiO$_2$ photoanode, Chemical Communications (2006) 4004–4006.
[34] M. Wang, N. Chamberland, L. Breau, J.-E. Moser, R. Humphry-Baker, B. Marsan, S.M. Zakeeruddin, M. Grätzel, An organic redox electrolyte to rival triiodide/iodide in dye-sensitized solar cells, Natural Chemistry 2 (2010) 385–389.
[35] Z. Zhang, P. Chen, T.N. Murakami, S.M. Zakeeruddin, M. Grätzel, The 2,2,6,6-tetramethyl-1-piperidinyloxy radical: an efficient, iodine-free redox mediator for dye-sensitized solar cells, Advanced Functional Materials 18 (2008) 341–346.